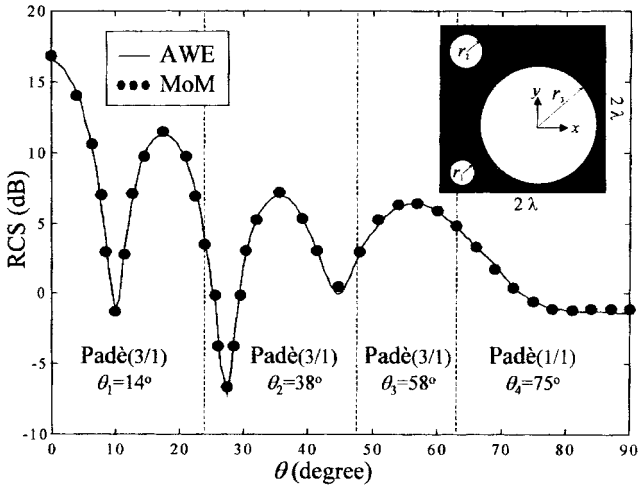

Fig. 1. Monostatic RCS pattern of a square metallic plate ($2\lambda \times 2\lambda$) with three circular slots ($r_1 = 0.15\lambda, r_2 = 0.25\lambda, r_3 = 0.7\lambda$): MoM (exact) versus AWE (approximate); multiple expansion points, $\theta_1 = 14°$, $\theta_2 = 38°$, $\theta_3 = 58°$ [Padè $(L = 3, M = 1)$], $\theta_4 = 75°$ [Padè $(L = M = 1)$].

of the CPU time used by the MoM. This comparison clearly shows how monostatic RCS patterns can be obtained much faster by means of AWE. Of course, as the number of angular points in the reference MoM solution increases, AWE becomes more attractive in terms of CPU cost.

To provide AWE users with some guidelines, we performed a systematic study of AWE order versus the angular band of the approximation. We observed that if one expansion point is chosen for every angular sector containing a single pattern lobe/null, a Padè approximation with $L = 1$, $M = 1$, or $M = 0$ results in a sufficiently accurate approximation. However, for angular sectors containing lobes and nulls, higher order expansions are necessary. For instance, expansions with (L/M) lower than $(3/1)$ for the first sectors of the example (see Fig. 1) would deteriorate the agreement.

III. Conclusion

In this letter, we presented an implementation of AWE for generating broad-band RCS patterns using only a few points of the exact solution. It was observed that AWE can result in considerable CPU time savings when an iterative solver is employed. We should point out that the accuracy and extrapolation range of the AWE implementation depend on several factors such as pattern shape, location of the expansion points, and the order of the Padè representation.

References

[1] E. K. Miller and G. J. Burke, "Using model-based parameter estimation to increase the physical interpretability and numerical efficiency of computational electromagnetics," *Computer Phys. Commun.*, vol. 68, nos. 1–3, pp. 43–75, Nov. 1991.

[2] S. Kumashiro, R. A. Rohrer, and A. J. Strojwas, "Asymptotic waveform evaluation for transient analysis of 3-D interconnect structures," *IEEE Trans. Computer-Aided Design*, vol. 12, pp. 988–996, July 1993.

[3] E. Chiprout and M. Nakhla, *Asymptotic Waveform Evaluation and Moment Matching for Interconnect Analysis*. Norwell, MA: Kluwer, 1994.

[4] J. Gong and J. L. Volakis, "AWE implementation for electromagnetic FEM analysis," *Electron. Lett.*, vol. 32, no. 24, pp. 2216–2217, Nov. 1996.

[5] M. A. Kolbehdari, M. Srinivasan, M. S. Nakhla, Q.-J. Zhang, and R. Achar, "Simultaneous time and frequency domain solutions of EM problems using finite element and CFH techniques," *IEEE Trans. Microwave Theory Tech.*, vol. 44, pp. 1526–1534, Sept. 1996.

[6] S. V. Polstyanko, R. Dyczij-Edlinger, and J.-F. Lee, "Fast frequency sweep technique for the efficient analysis of dielectric waveguides," *IEEE Trans. Microwave Theory Tech.*, vol. 45, pp. 1118–1126, July 1997.

The Diffraction of an Inhomogeneous Plane Wave by an Impedance Wedge in a Lossy Medium

Giuliano Manara, Paolo Nepa,
Robert G. Kouyoumjian, and Barendt J. E. Taute

***Abstract*— The diffraction of an inhomogeneous plane wave by an impedance wedge embedded in a lossy medium is analyzed. The rigorous integral representation for the field is asymptotically evaluated in the context of the uniform geometrical theory of diffraction (UTD) so that the asymptotic expressions obtained can be employed in a ray analysis of the scattering from more complex edge geometries located in a dissipative medium. Surface wave excitations at the edge and their propagation along the wedge faces are discussed with particular emphasis on the effects of losses.**

***Index Terms*—Absorbing media, electromagnetic scattering, wedges.**

The diffraction of an inhomogeneous plane wave by an impedance wedge embedded in a lossy medium is considered in this letter. The uniform analysis presented in [1] for a perfectly conducting wedge is extended here to the case in which impedance boundary conditions (IBC's) occur at both faces of the wedge to account for its material properties. The aim is to extend the uniform geometrical theory of diffraction (UTD) to this case. We note that a uniform plane wave impinging on the interface between air and a lossy medium gives rise to an inhomogeneous plane wave in the lossy medium; consequently, the above problem is important in the analysis of electromagnetic scattering from buried objects.

The geometry for the two-dimensional scattering problem is depicted in Fig. 1, where all the parameters are defined as in [1]. The edge of the wedge is positioned on the z axis and the observation point P is located at ρ, ϕ in the polar coordinate system. The two faces of the wedge ($\phi = 0$ and $\phi = n\pi$) are characterized by different surface impedances Z_0 and Z_n, respectively. In the following, both polarizations are treated at the same time, i.e., the total field u may denote either H_z in the TE (hard) case or E_z in the TM (soft) case. An $\exp(j\omega t)$ time dependence is assumed and suppressed. Since the medium surrounding the wedge is lossy the wave number $k = \beta - j\alpha$ is complex. The incident inhomogeneous plane wave exhibits both a real $(\mathbf{k}')$ and an imaginary $(\mathbf{k}'')$ wave-vector component; the angle between the two is $\Omega < \pi/2$, shown in Fig. 1. As described in [1], the

Manuscript received January 26, 1998.

G. Manara and P. Nepa are with the Department of Information Engineering, University of Pisa, Pisa, I-56126 Italy.

R. G. Kouyoumjian is with the ElectroScience Laboratory, The Ohio State University, Columbus, OH 43210 USA.

B. J. E. Taute is with the Manufacturing and Aeronautical System Technology, CSIR, Pretoria, 0001 South Africa.

Publisher Item Identifier S 0018-926X(98)08902-9.

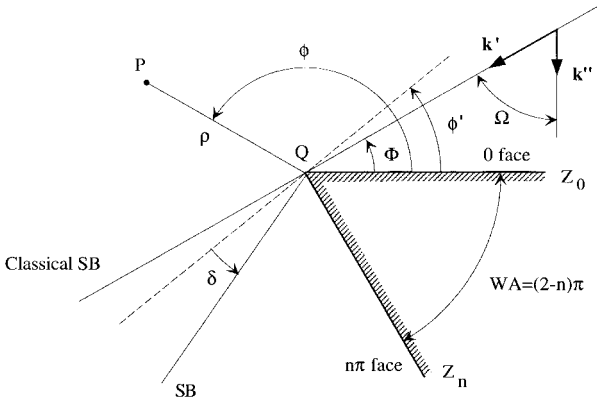

Fig. 1. Geometry for the scattering problem.

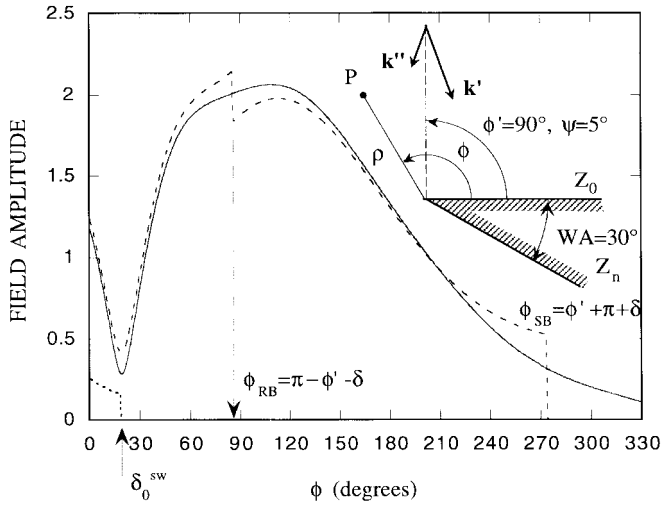

Fig. 2. Field amplitude versus the observation angle ϕ for the TE case: GO contribution (dashed line), surface wave contribution (dotted line), and total field (continuous line). Geometrical and electrical parameters: $n = 11/6$, $\phi' = 90°$, $\psi = 5°(\delta = 4.06°)$, $\sin\theta_0 = 0.1 + j0.54(\delta_0^{\rm sw} = 18.5°)$, $\sin\theta_n = 0.1 - j0.54$.

incident field $u^i = \exp\{jk\rho\cos[\phi-(\phi'-j\psi)]\}$ can be interpreted as a uniform plane wave impinging on the edge with a complex angle of incidence $\phi' - j\psi$.

A rigorous spectral integral representation for the total field in the presence of an impedance wedge has been given by Maliuzhinets in [2]

$$u(\rho,\phi) = \frac{1}{2\pi j}\int_\gamma G(\xi+\phi-n\pi/2)e^{jk\rho\cos\xi}\,d\xi \tag{1}$$

which is valid also for complex incidence angles. In (1), $\gamma = C' - C$ is the standard Sommerfeld integration path shown in [1, Fig. 2] and

$$G(\xi) = \frac{M(\xi)}{M(\phi' - j\psi - n\pi/2)}\sigma(\xi) \tag{2}$$

where $\sigma(\xi)$ is a trigonometric function containing the geometrical optics (GO) poles and $M(\xi)$ is the Maliuzhinets special function.[1] Both $\sigma(\xi)$ and $M(\xi)$ are defined in [2], where a summary of the properties of the Maliuzhinets special function is also given. We note that due to the use of a different coordinate system, in the expressions in [2] Φ, φ, and φ_0 must be replaced by $n\pi/2$, $\phi - n\pi/2$, and $\phi' - j\psi - n\pi/2$, respectively. Also, i in [2] must be replaced by $-j$ because of the different time convention. $M(\xi)$ depends on the Brewster angles θ_0 and θ_n of the face $\phi = 0$ and $\phi = n\pi$, respectively. These latter are defined by $\sin\theta_{0,n} = Z_{0,n}/\zeta$ in the TE (hard) polarization case and $\sin\theta_{0,n} = \zeta/Z_{0,n}$ in the TM (soft) polarization case, where ζ is the characteristic impedance of the medium surrounding the wedge, which is complex in the case of a lossy medium. Several approximations of $M(\xi)$, which are suitable for its efficient calculation have been proposed in the literature (see [3] and its bibliography).

The procedure for deriving a uniform asymptotic expression for the total field is the same as that adopted in [1], except for the presence of the surface wave poles. As far as the GO fields are concerned, the presence of the IBC's at the wedge faces simply implies multiplying each reflected field contribution by the reflection coefficient of the pertinent face. Since the regions of existence of the GO fields are not affected by the IBC's at the wedge faces, the displacement δ (see Fig. 1) of the shadow (SB) and reflection (RB) boundaries from their conventional locations is the same as that given in [1]. Moreover, the surface wave contributions at the faces $\phi = 0$ and $\phi = n\pi$ can be written as $u_0^{\rm sw} = C_0\exp\{-jk\rho\cos(\phi+\theta_0)\}$ and $u_n^{\rm sw} = C_n\exp\{-jk\rho\cos(\phi - n\pi - \theta_n)\}$, where C_0 and C_n equal C_- and C_+, respectively, in [2]. We note that due to the presence of losses in the medium surrounding the wedge, a surface wave excited at the edge and propagating along a face is attenuated, even when the face exhibits a purely reactive surface impedance. This effect may be important in the scattering from structures with edges located in lossy media, if it significantly reduces the contributions to the scattered field from surface wave excitation and diffraction. Note that these contributions can be calculated from this solution. When the exterior medium is lossy, the shapes of the two steepest descent paths (SDP's) shown in [1] are changed and both the surface wave excitations and the extent of their lit regions are modified with respect to those given in [2]. The lit regions are defined by $0 \le \phi \le \delta_0^{\rm sw}$ for the face $\phi = 0$ and $n\pi - \delta_n^{\rm sw} \le \phi \le n\pi$ for the face $\phi = n\pi$, where

$$\delta_{0,n}^{\rm sw} = \sin^{-1}\left\{\sqrt{1-(\alpha/\beta)^2}\,\frac{\tanh[{\rm Im}(\theta_{0,n})]}{1+\alpha/\{\beta\cosh[{\rm Im}(\theta_{0,n})]\}}\right\} - {\rm Re}(\theta_{0,n}) \tag{5}$$

with the excitation condition requiring $\delta_{0,n}^{\rm sw} > 0$. It is evident that ${\rm Im}(\theta_{0,n})$ must be positive for a surface wave to exist.

Finally, employing the same asymptotic evaluation of the integrals along the SDP's through the saddle points at $\xi = \pm\pi$ adopted in [1], we obtain the following uniform expression for the diffracted field:

$$u^d \sim -\frac{e^{-j\pi/4}}{\sqrt{2\pi k}}\left\{G(\pi+\phi-n\pi/2) - G(-\pi+\phi-n\pi/2) - \sum_p {\rm Res}[G(\xi),\xi=\xi_p] \times \frac{1-F\left[\sqrt{k\rho[1+\cos(\xi_p-\phi+n\pi/2)]}\right]}{2\cos[(\xi_p-\phi+n\pi/2)/2]}\right\}\frac{e^{-jk\rho}}{\sqrt{\rho}} \tag{6}$$

where the summation includes both the GO poles and the surface wave poles at $\xi = \xi_p$ when these poles lie either between the two SDP's shown in [1, Fig. 2] or in the complementary exterior region of the complex ξ plane, but at a distance from the closest SDP (measured along the real axis) less than π. See the discussion in [1, Sec. 4.2]. $F[\cdot]$ is the UTD transition function extended to complex arguments.

A sample of numerical results is shown in Fig. 2, where the amplitude of the GO field contribution, the surface wave contribution and the total field at a constant distance ($\rho = \pi/|k|$) from the edge of an impedance wedge are plotted as functions of the observation angle ϕ. The lossy medium surrounding the wedge is characterized

[1] Note that the Maliuzhinets function is usually denoted by $\Psi(\xi)$.

by $\beta/|k| = 0.98$ and $\alpha/|k| = 0.199$. Because of the values chosen for the Brewster angles, only the face $\phi = 0$ supports a surface wave. It is apparent that the total field pattern is smooth and continuous, as expected from a uniform asymptotic solution. To check the accuracy of this calculation, a direct numerical evaluation of the rigorous Maliuzhinets representation along the SDP's was carried out. The resulting pattern was found to superimpose exactly on that shown in Fig. 2.

REFERENCES

[1] R. G. Kouyoumjian, G. Manara, P. Nepa, and B. J. E. Taute, "The diffraction of an inhomogeneous plane wave by a wedge," *Radio Sci.*, vol. 31, no. 6, pp. 1387–1397, Nov./Dec. 1996.

[2] G. D. Maliuzhinets, "Excitation, reflection and emission of surface waves from a wedge with given face impedances," *Sov. Phys. Dokl.*, vol. 3, pp. 752–755, 1958.

[3] J. L. Hu, S. M. Lin, and W. B. Wang, "Calculation of Maliuzhinets function in complex region," *IEEE Trans. Antennas Propagat.*, vol. 44, pp. 1195–1196, Aug. 1996.

Calculation of Diffraction Coefficients of Three-Dimensional Infinite Conducting Wedges Using FDTD

Veeraraghavan Anantha and Allen Taflove

***Abstract*—The finite-difference time-domain (FDTD) method is applied to obtain the three-dimensional (3-D) dyadic diffraction coefficient of infinite right-angle perfect electrical conductor (PEC) wedges illuminated by a plane wave. The FDTD results are in good agreement with the well-known asymptotic solutions obtained using the uniform theory of diffraction (UTD). In principle, this method can be extended to calculate diffraction coefficients for 3-D infinite material wedges having a variety of wedge angles and compositions.**

***Index Terms*—Electromagnetic scattering, FDTD methods.**

We extend the two-dimensional (2-D) approach discussed in [1] to obtain numerically the three-dimensional (3-D) dyadic diffraction coefficients for right-angle perfect electrical conductor (PEC) wedges. This method exploits the temporal causality inherent in finite-difference time-domain (FDTD) modeling. In principle, this method can be extended to calculate diffraction coefficients for 3-D infinite material wedges having a variety of wedge angles and compositions.

Diffraction from a PEC wedge illuminated by an obliquely incident plane wave can be described by a dyadic diffraction coefficient [2]. By choosing the appropriate ray-fixed coordinates [Fig. 1(a) and (b)], the diffraction coefficient is described as a sum of two dyads [2], which, in matrix notation, is represented by a diagonal 2×2 matrix. The two nonvanishing elements are the soft and the hard scalar diffraction coefficients D_s and D_h. Fig. 1(a) shows the edge-fixed plane of incidence $(\hat{s}', \hat{e})$ with the ray-fixed unit vectors $\hat{\beta}_0'$ and $\hat{\phi}'$ parallel and perpendicular to it, respectively. Also shown is the edge-fixed plane of diffraction $(\hat{s}, \hat{e})$ with the ray-fixed unit vectors $\hat{\beta}_0$ and $\hat{\phi}$ parallel and perpendicular to it, respectively. The radial unit vectors of incidence and diffraction are given by $\hat{s}' = \hat{\phi}' \times \hat{\beta}_0'$ and $\hat{s} = \hat{\phi} \times \hat{\beta}_0$.

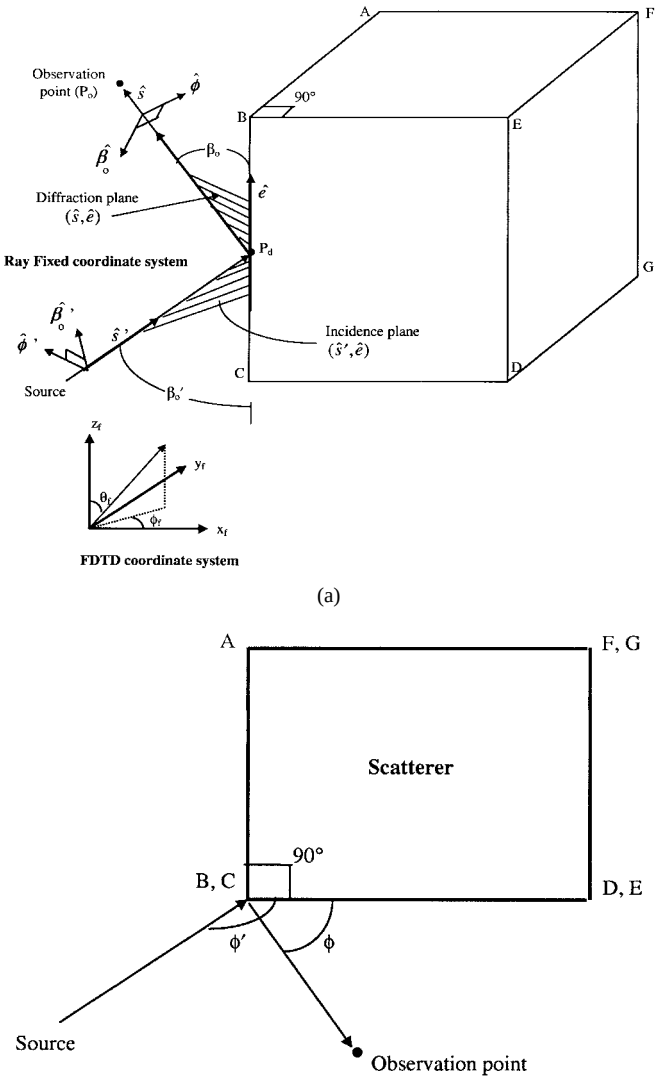

Fig. 1. (a) Three-dimensional geometry of the PEC scatterer showing the edge-fixed plane of incidence and diffraction, the ray-fixed coordinate system, and the FDTD coordinate system. (b) Top view of the scattering edge showing the angles made by the projections of the incident and diffracted wavevectors in plane ABEF.

In order to obtain the numerical dyadic diffraction coefficient, we first find the diffracted-field impulse response of the scatterer numerically using FDTD. By illuminating the wedge with a pulsed plane wave having an electric field (E-field) component parallel to the plane of incidence, we obtain the diffracted-field impulse response $h_{\beta_0,\mathrm{num}}$ polarized parallel to the plane of diffraction. An analogous procedure is performed with the incident E-field component perpendicular to the plane of incidence, yielding $h_{\phi,\mathrm{num}}$ polarized perpendicular to the plane of diffraction. The Fourier transforms of these diffracted-field impulse responses $H_{\beta_0,\mathrm{num}}$ and $H_{\phi,\mathrm{num}}$, give the corresponding spectra of the diffracted fields. D_s

Manuscript received March 20, 1998; revised July 21, 1998.

V. Anantha is with the Cellular Infrastructure Group, Motorola Inc., Arlington Heights, IL 60004 USA.

A. Taflove is with the Department of Electrical and Computer Engineering, Northwestern University, Evanston, IL 60208 USA.

Publisher Item Identifier S 0018-926X(98)08903-0.